Interaction mechanisms between Atomic Oxygen and materials: investigation on reflected beam

David Leveque, Sophie Duzellier, Meggie Vilaranda Fernandes, Guilhem Chanteperdrix, David Nguyen van Sang, Véronique Perrin-Bailly, Pierre Jouanne, E Laurent

Interaction mechanisms between Atomic Oxygen and materials: investigation on reflected beam

Interaction mechanisms between Atomic Oxygen and materials: investigation on reflected beam

D Leveque[1], S Duzellier[1], M Vilaranda Fernandes[2], G Chanteperdrix[2], D Nguyen Van Sang[3], V Perrin-Bailly[3], P Jouanne[3], E Laurent[4]

[1] ONERA/DPHY, Université de Toulouse, F-31055 Toulouse - France
[2] AIRBUS DEFENCE AND SPACE, 31 Rue des Cosmonautes, 31400 Toulouse, France
[3] THALES ALENIA SPACE, 5 Allée des Gabians, 06150 Cannes, France
[4] Sous-direction Qualité Expertise, Service Technologies, Matériaux et Procédés, CNES, 18 avenue Edouard Belin, 31401 Toulouse Cedex 9, France

E-mail: david.leveque@onera.fr

Abstract. Atomic Oxygen (AO) is the main component of the residual atmosphere present at low earth orbit. Multiple reflections can locally enhance or lower erosion rate in case of complex geometry. The need for precise estimate of hyperthermal AO flux is thus crucial at critical target embedded into realistic assembly. Industrial modeling tools (example Atomox module in ESABASE2 and SYSTEMA toolboxes) may account for multiple reflections with simplistic approach (ray-tracing) and a set of semi-empirical parameters. In this context, an original geometrical setup was designed in order to expose target surfaces with normal and tilted incidences and after one reflection on a set of materials of interest (black conductive thermal coatings, coverglass, surface treatment…). Candidate materials have been selected in view to compare numerical results and experimental ones. Results of two test campaigns highlight the effect of incidence angle on erosion rate (higher erosion with tilted beam) and provide an estimate of residual fluence after one reflection (in the 4-10 % range depending on material type). First computations with engineering codes have been successfully conducted, the erosion patterns being rather well described with some basic hypotheses on material parameters (absorption, specular/diffuse reflection) and taken into account the reflection on adjacent metallic surfaces.

1. Introduction

Atomic oxygen (AO) is the main component of the residual atmosphere present at low earth orbit [1]. AO is considered as one of the most serious hazards to spacecraft materials. The main consequence is oxidation and erosion of surface materials. Some classes of materials are stable under AO attack (oxides for instance) and incoming flux is then re-emitted with specific angular and energy distributions. The response to AO of space materials is known via measurement of the erosion yield. Multiple reflections can locally enhance or lower erosion rate in case of complex geometry.

The issue of materials erosion by AO is mainly considered in a worth case manner i.e. with an AO flux fully directed towards exposed surface. Nevertheless in some critical applicative cases, the local geometry of sub-system may be complex (for instance: optical devices with baffles, surfaces in sight of solar panels …) where phenomena of oxygen atoms diffusion/reflection/absorption can take place, and can lead to erosion of surfaces without direct exposure to space environment [2].

The need for precise estimate of hyperthermal AO flux is crucial for critical target embedded into a complex geometry. Depending on the configuration, target can be partially masked or exposed to additional AO flux due to scattering. Scattering mechanisms have been reported for instance in flight data [3][4] and at ground studies [5].

Modeling tools (example Atomox module in ESABASE2 and SYSTEMA industrial frameworks) may account for multiple reflections with simplistic approach (ray-tracing) and a set of semi-empirical parameters.

In this context, an original geometrical setup was designed in order to expose target surfaces with normal incidence or after one reflection. Experimental investigation was carried out to study the effect of hyperthermal AO in case of complex geometry and estimate the "secondary" AO flux after reflection on selected set of targets. At last a comparison was made between experimental observations and calculations of AO erosion in case of such scattered AO mechanisms. Preliminary results presented in [6] are completed and detailed in this paper.

2. Test approach and ground experiments

2.1. Geometry design

Ground experiment of AO multi-reflection effect can be found in the literature and address different thematic and objectives:

- Investigation of local erosion enhancement linked to chamfered geometries (edge effect, [7]),
- Develop mitigation and attenuation approach to secondary thermal AO beams [8],
- In [5], reflection jig was used to measure the ratio of reflected component at different angle.

Similarly, we designed and developed an original setup to expose target surfaces with normal incidence or after one reflection (Figure 1). First, the geometry was designed in order to be able to expose at the same time different materials in normal (position 1 to 3) and inclined positions (position 4). The angle of inclination in our case is 65° between the main flux direction and the normal of the surface. At position number 5, a detector is placed in such manner it is hidden from the main flux but receive the reflected flux from the inclined material. Positions 3 and 4 are fitted with candidate materials whose erosion yields at normal and tilted incidence can be measured based on mass loss measurement. The configuration of the assembly also generates AO scattering on part 4 and detection of scattered flux at position 5 (reference kapton foil with known erosion yield, or active Resistack detector [9]). At position 5, it comes an estimate of the ratio of reflected AO flux received by the detector. Lastly, reference Kapton foil (position 1) is used for the measurement of the fluence level in primary (normal) beam. In practise, the Kapton erosion yield is independent of the macroscopic incident angle, using the $\cos(\theta)$ correction [10]. Position 2 is used for any additional material.

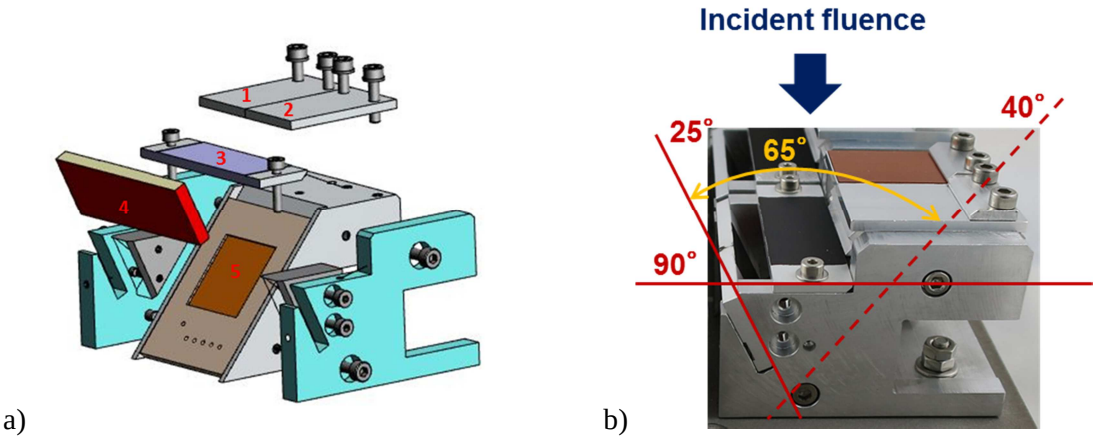

a) b)

Figure 1. a. geometry design (exploded view). **b.** assembled geometry with orientation references.

2.2. Materials choice

In terms of materials choice, Kapton HN film is used as a test-fluence standard, like proposed by Minton [11]. At position 1, the local incident fluence is estimated for each geometry. At position 5, the residual fluence after reflection is also estimated by measuring the mass loss and knowing the erosion yield of Kapton.

The materials under test are composed of black conductive thermal coatings (BCTC1, BCTC2 and BCTC3), a plasma chemical coating (PCC), a polyimide film like kapton (KAP), a coverglass (CVG) and an aluminized Kapton films too. Due to confidentiality purpose, only the generic family is indicated for each material.

All materials under test (MUT) samples have their witness samples, i.e. samples of same geometry and same nature but that are kept safely in a dry and neutral environment, used as a reference for mass loss measurement.

2.3. Test setup

Two Atomic Oxygen exposure campaigns were conducted at LEOX facility in the ESA-ESTEC laboratory (figure 2a), with a first screening test campaign (selection of materials) with a low fluence (~$2x10^{20}$ atoms/cm²), and a second test campaign with higher fluence (~$2x10^{21}$ atoms/cm²). The LEOX facility has a source concept based on the Laser Pulse Induced Breakdown (LPIB) principle with an AO hyperthermal energy of ~ 5 eV (relative velocity of about 8 km/s). Figure 2b depicts the sample holder of this second test campaign with the associated selected materials shared between six different geometries.

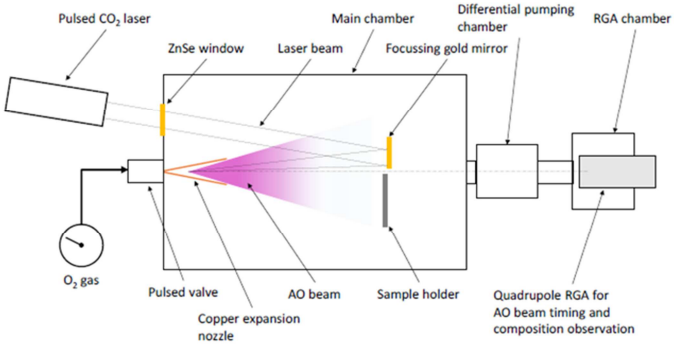

a)

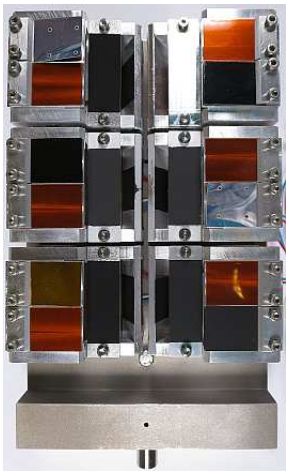

b)

Figure 2. a. Schematic of the LEOX facility (ESA-ESTEC). **b.** LEOX2 sample holder before AO exposure test.

Before and after each test campaign, all the material samples are dried and weighted following the procedure detailed in [11]. From the mass loss, one can easily determine the erosion yield knowing the exposed surface area, the MUT density and the local incident fluence. The local incident fluence is estimated on each geometry thanks to the reference Kapton foil (located at position 1) from its mass loss and its well-known erosion yield ($3.0\ 10^{-24}$ cm3/atom). Due to the wide discrepancy of the incident fluence level over the sample holder from one side to another, the fluence level was interpolate on all the exposed surfaces in order to better estimate the incident fluence associated with each MUT sample. Moreover, from this mapping the mean global fluence can be estimated over the whole holder plate at ~$1.7\text{x}10^{20}$ atoms/cm² for LEOX1 and ~$2.4\text{x}10^{21}$ atoms/cm² for LEOX2 test campaigns.

3. Test preliminary results

3.1. Erosion rates

Figure 3 discloses the normal-to-tilted erosion yield ratio for the set of materials under test. This is the ratio of the normal erosion yield to the erosion yield measured with an impingement angle θ ($\theta = 65°$ in our case). For these estimations, the effective fluence was used, *i.e.* corrected by the $\cos(\theta)$ factor. When this ratio is equal to unity, the erosion yield is independent on the impingement angle. The standard deviation estimated on each ratio value includes the standard deviation due to the measurement of mass loss and exposed area surface (erosion yield calculation) as well as the incident fluence estimation (residual of fluence mapping).

At first, it is confirmed the absence of angle influence on the erosion yield of Kapton HN considering the proposed $\cos(\theta)$ correction [10]. For the other MUT samples, this ratio is much lower than 1 showing higher erosion yield for all tilted samples whatever the material family and type tested in this study. It should not be always the case, as some other works have measured a strong material-dependent erosion yield ratio, this ratio could be even greater than 1 [12].

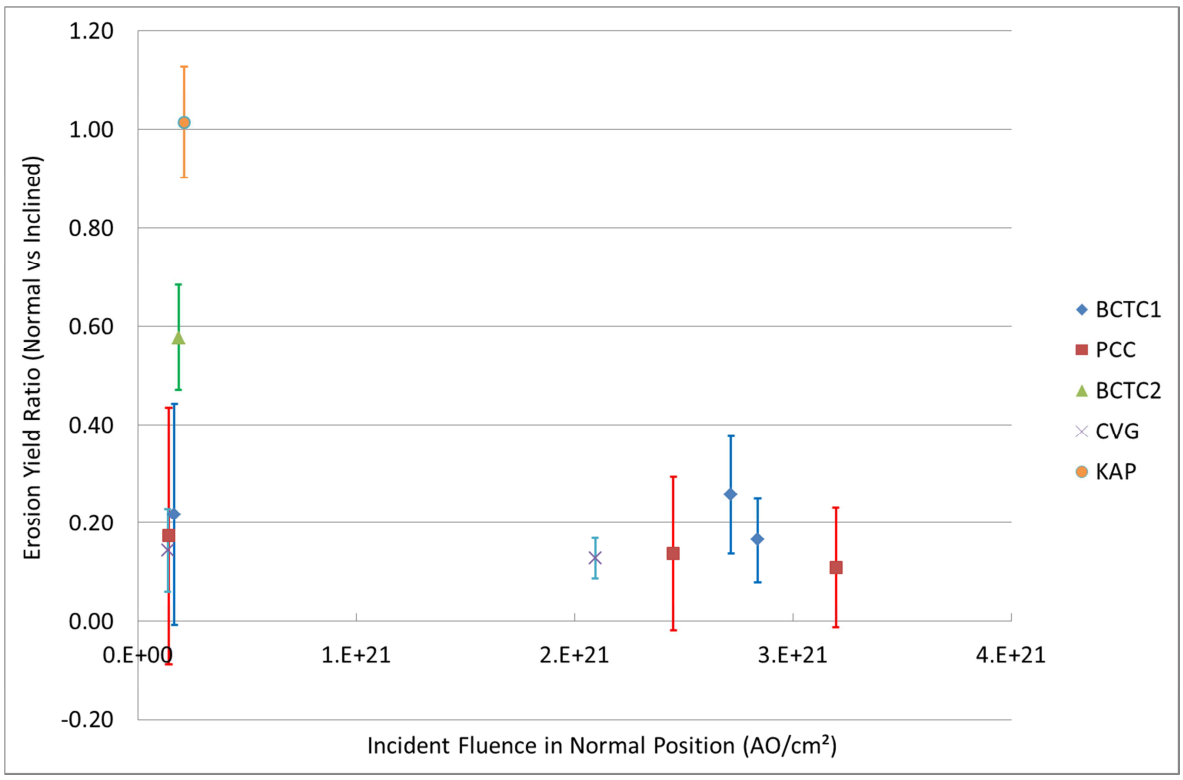

Figure 3. Erosion yield ratio (ratio of normal erosion yield to tilted erosion yield).

3.2. Residual fluences after reflection

The values reported in Table 1 correspond to the proportion (in percent) of incident fluence resulting in erosion of Kapton HN foils (used in the detection plane) after reflection on the MUT surfaces. Secondary-to-primary flux ratio ranges in the 4-10 % values that are of the order of magnitude of data reported in [5] or [8] (at a different reflection angle and for different materials). This secondary fluence estimation is consistent between LEOX1 and LEOX2 campaigns (BCTC1, CVG and PCC comparison in Table 1) even with a lower fluence level (one order of magnitude) in the first case.

Table 1. Secondary fluence comparison.

	Secondary fluence (%)	
Reflector material	LEOX1	LEOX2
BCTC1	4	5
BCTC2	7	-
CVG	9	10
KAP	6	-
PCC	7	8
BCTC3	-	10
AL	7	-

3.3. Erosion observations

In terms of AO erosion analysis, several observations were conducted. The first one is a visual inspection (optical) of the Kapton film detectors. By optical contrast, we can see interesting erosion feature as disclosed in Figure 4b for PCC sample and in Figure 5 for all samples:

- Erosion area can be observed and measured. The area between the two yellow dash lines in Figure 5 corresponds to the theoretical specular zone, *i.e.* with same incident and reflected angles (see Figure 4a), well defined geometrically speaking (5.3 mm in height in our case; Figure 4a).
- Clearly both specular and diffuse components add to the overall erosion of Kapton HN. Specular and diffuse response surface is lower than theoretical total exposed surface (not masked, see Figure 4b).

Observation of Kapton detectors for all MUT samples shows specific material-dependent signature. For instance, similar ratios of secondary fluence were measured for PCC and CVG (resp. 8 and 10 %; Table 1) but the feature of visible eroded areas are very different with (Figure 5):

- A total eroded zone much larger for PCC,
- Eroded zone limit is rather concave for CVG, straight for PCC.

For BCTC1 reflector material, the eroded area limit is rather concave like CVG material; for the BCTC3 material, the limit is rather straight and the diffuse erosion seems more extended like in the PCC case.

Figure 4. a. Reflection angles inside a geometry. **b.** Optical observation of erosion areas for PCC sample.

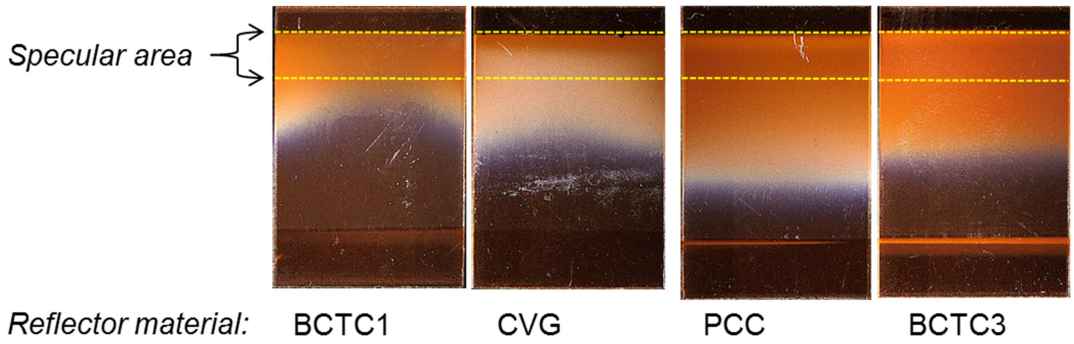

Figure 5. Optical observation of LEOX2 Kapton film detectors exposed to MUT scattered beam.

The second observation corresponds to the investigation of the eroded surfaces by SEM. The Figure 6 depicts the particular case of the Kapton film detector exposed to the BCTC3 reflector material. The total theoretical exposed area is defined between the two dash lines. The Z1 area corresponds to the specular reflection, with a canyon-like eroded facies but with rather smooth peaks (Figure 7). The highest peaks under localized dust give an idea of the erosion depth. In the pure diffuse area Z2, the erosion depth is weaker and the Z3 area, without optical contrast, seems not affected by

the erosion. One should note in the extreme border Z1' the erosion is well marked with higher peaks, probably due to a concentration effect (see next paragraph), as suggested by Banks and Miller [7].

Figure 6. Kapton film detector exposed to reflected flux of BCTC3 sample: definition of the different zones of SEM observations (Figure 7).

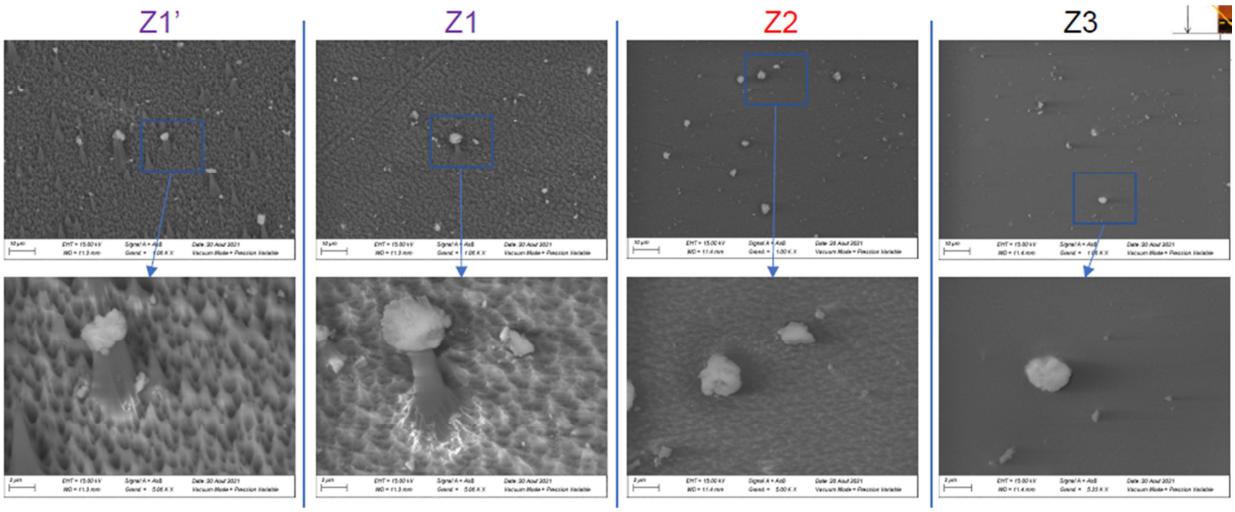

Figure 7. Different zones of SEM investigation on Kapton film detector surface (BCTC3 reflector).

These observations were followed by complementary profilometry measurements conducted with a 3D optical profilometer. For the same film detector of Figure 6, the profilometry measurement is compared to the optical observation at Figure 8. The optical observation is reported here with an amplified length scale and compared to the profilometry realized along the median line (in white). In the specular area (at left of the specular/diffuse border) the profile of erosion is more perturbed and in the diffuse area the profile is smoother. We retrieve the amplified erosion depth located at the two extremities of the exposed surface (arrows), as suggested by Banks and Miller [7] it's identified as a sample holder edge effect.

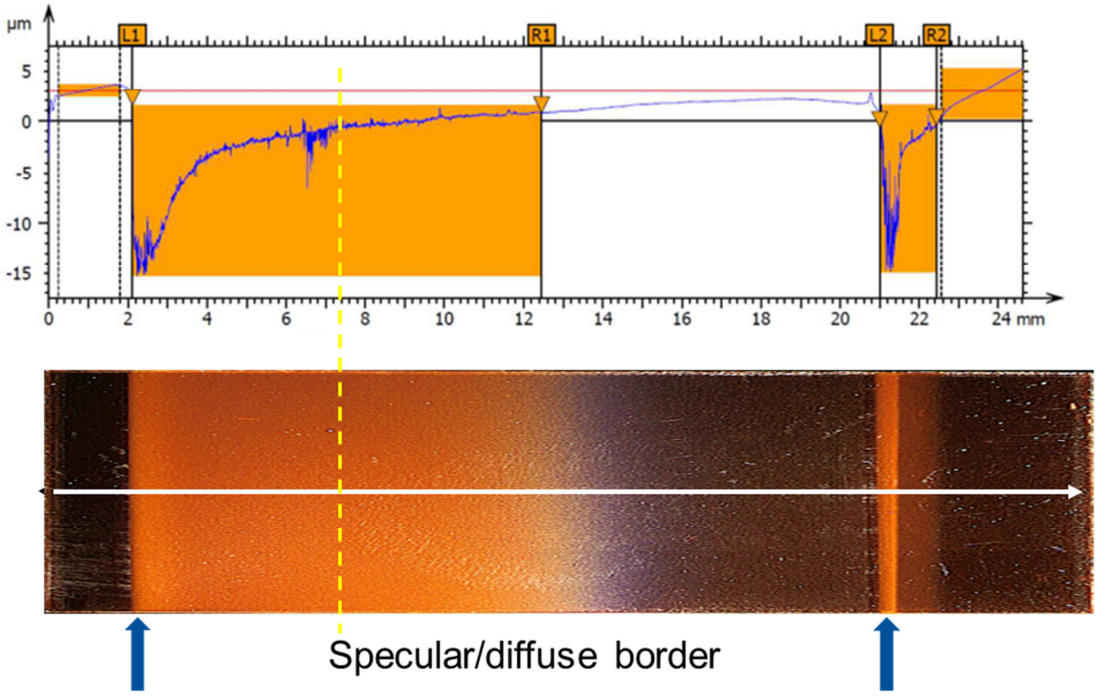

Figure 8. Optical observation vs profilometry: KAP-F-2 detector (BCTC3 reflector).

4. Modelling with engineering tools

4.1. Background and inputs for calculations

ESABASE2 and Systema-Atomox is using the ray-tracing technique which is well adapted for treating multiple-reflections. The method is summarized by the following. For a ray carrying N number of particles (Figure 9):

- Part of this number is absorbed by the surface, such as $N_a = \Omega N$,
- Part of this number is specularly reflected, such as $N_s = S_r N$, S_r being the specular reflection coefficient,
- Part of this number is diffusely reflected in a defined number of rays Lambert's cosine law, such as $N_d = S_d N (1\text{-}R)$, S_d being the diffuse reflection coefficient and R the accommodation ratio.

These coefficients are linked by the relationship: $\Omega + S_r + S_d = 1$.

To use the ATOX module, the user has to define a set of 4 parameters for each material:

- Ω, the absorption coefficient,
- The specularity ratio S, such as $S = \frac{Sr}{Sr+Sd}$,
- The accommodation ratio R in case of diffuse reflection,
- The (known) erosion rate.

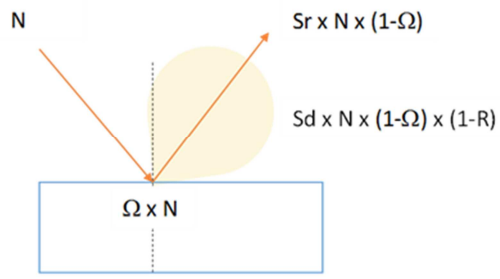

Figure 9. Main parameters of ATOMOX model.

Due to the complexity of the actual geometry and non-perfect material surfaces, several hypotheses are here considered:

- Hard-cube model, i.e. the reflected angle is the same than the incident one,
- No roughness of the target plane taken into account,
- No thermal motion,
- No accommodation, hence r = 0,
- Using this method, one can deduce that for a ray carrying N number of particles and hitting a surface, the particle conservation gives $N = N_a + N_s + N_d$,
- Multiple-reflection authorized but primary reflection results mainly observed,
- Estimate of the parameters for Kapton film detector can be deduced from the literature [13][14], with $\Omega = 0.15$ and $S = 0.5$.

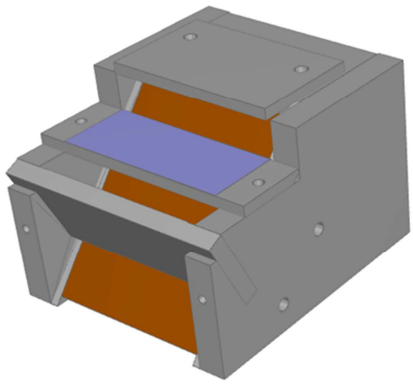

Figure 10. Geometrical model.

Figure 10 is a representation of the model of the experimental geometry used. It has been decided to check if the eroded patterns of Figure 5 could be numerically reproduced with some basic hypotheses.

4.2. Boundary cases simulations

It is first important to check if the specular zone's height of 5.3 mm is reproduced numerically.
To do so, let us consider a fully specular material. With the engineering tool, the eroded zone on the sensor is shown in Figure 11. Here the specular zone corresponds to the red rectangle. Its height is about 5.4 mm.

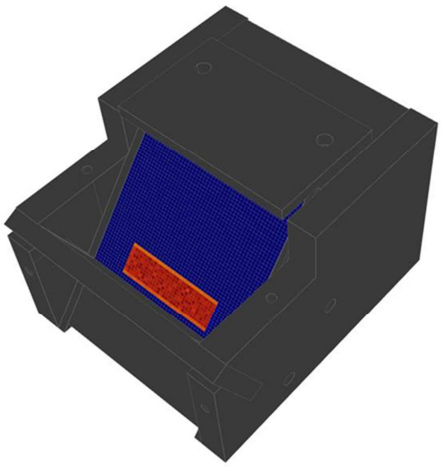

Figure 11. Eroded area in case of a fully specular material.

After the specular zone check, a fully diffusive material has been computed to see if the different eroded patterns of Figure 5 could be explained by a diffuse material. The eroded zone on the sensor is shown at Figure 12. According to the pattern of this fully diffusive material, the experimental eroded patterns which show higher erosion levels on the sides than at the center (especially BCTC1 and CVG) cannot be fully explained by diffusive materials in simulations. When examining the test geometry, one can observe that the samples don't fully cover the support (Figure 13a). One explanation of the eroded pattern could then be the diffusive reflection of the metallic support (aluminum material).

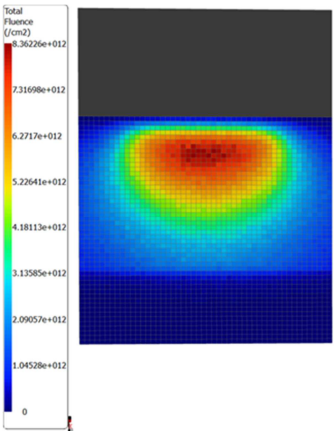

Figure 12. Eroded area in case of a fully diffuse material.

According to a simulation, in case of diffusive metallic surfaces of the side of the samples, the eroded pattern corresponding to these surfaces alone are as shown below (Figure 13b). It is then suggested that the eroded patterns obtained are due to the diffusive reflection of the metallic surfaces which is added to the AO reflections on the MUT samples.

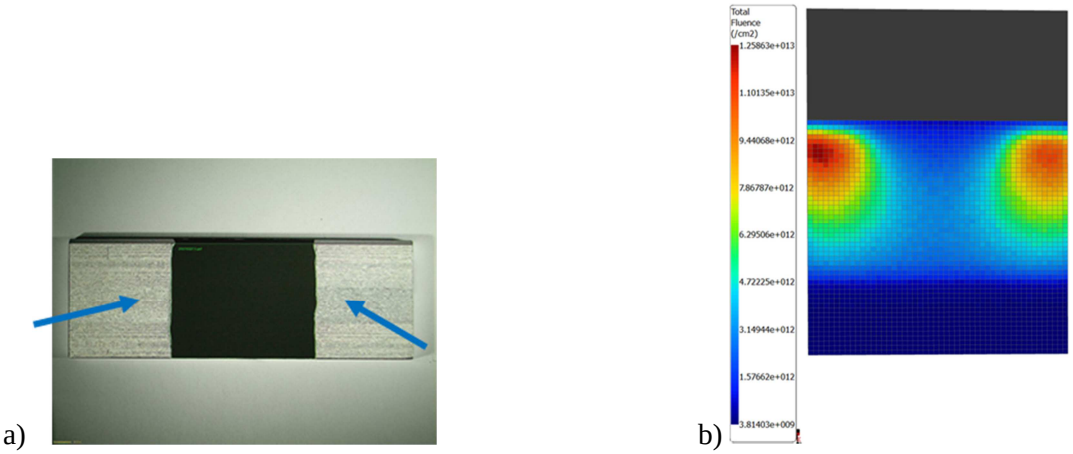

Figure 13. a. Inclined MUT sample with aluminium support. **b.** Computed eroded pattern due to metallic sides diffusion.

4.3. First comparison with experimental results

Because of the supposed contribution of metallic parts, a new set of parameter has to be determined. To do so, it is decided to suppose that the BCTC1 is a specular material and thus the erosion observed on the sides (Figure 14) should mainly be due to the metallic parts. Indeed, to determine a set of parameters thanks to analytical equations (estimation of reflected fluences), points of control have to be defined (see Figure 14). It is first arbitrary chosen to put the eroded level of the "white" blurry line to a corresponding erosion depth of Kapton of 2 μm. With this hypothesis, one can decouple the analytic equations of the two different kind of materials. Using this method, metallic sides parameters are put at $\Omega = 0.12$ and $S = 0.08$ in our simulations.

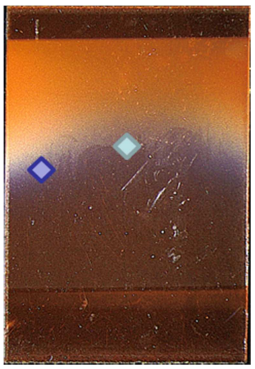

Figure 14. Points of control used for BCTC1 material.

Using the same reasoning, one can approximate the samples' set of parameters (see Table 2) using this point of control considering the hypothesis on the eroded level at the "white line" at 2 μm. To numerically recreate the eroded pattern, the calculated points of control have been taken in the middle of the top side (Figure 14) because according to Figure 5, erosion levels coming from metallic surfaces are lower here, so less perturbation is introduced.

Table 2. Estimation of MUT samples' set of parameters.

MUT sample	BCTC1	CVG	PCC	BCTC3
Ω	0.85	0.82	0.73	0.75
S	0.52	0.45	0.3	0.37
S_r	0.078	0.081	0.081	0.0925
S_d	0.072	0.099	0.189	0.1575

With this set of parameters, computed eroded patterns are compared to the experimental observations for a rather specular material (BCTC1) at Figure 15 and for a rather diffuse material (PCC) at Figure 16. One should note in the following simulations, the incident fluence has been set to the same value of 2.47 10^{21} at/cm² for all geometries.

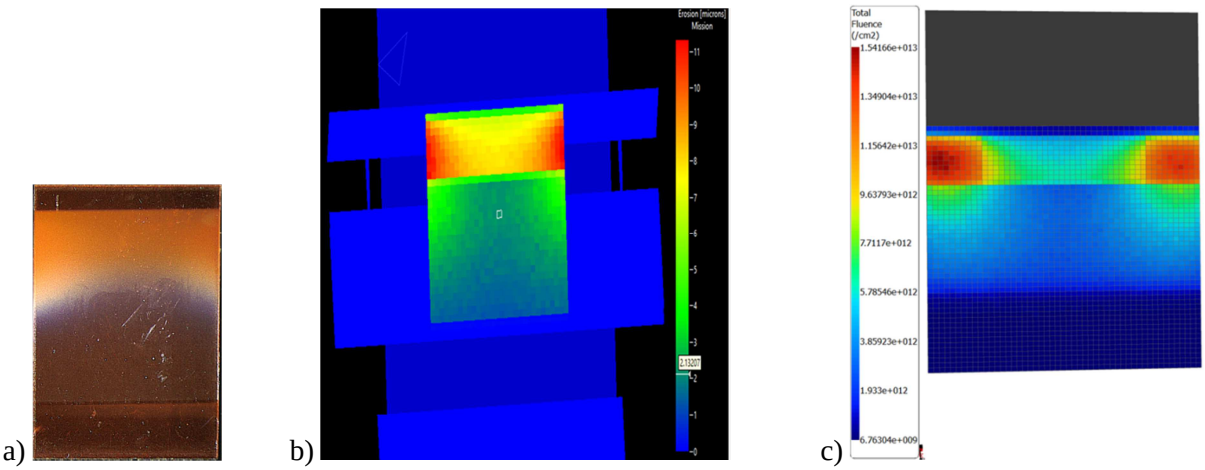

Figure 15. a. Optical eroded pattern (BCTC1 reflector). Computed eroded pattern (**b**: ESABASE2; **c**: SYSTEMA).

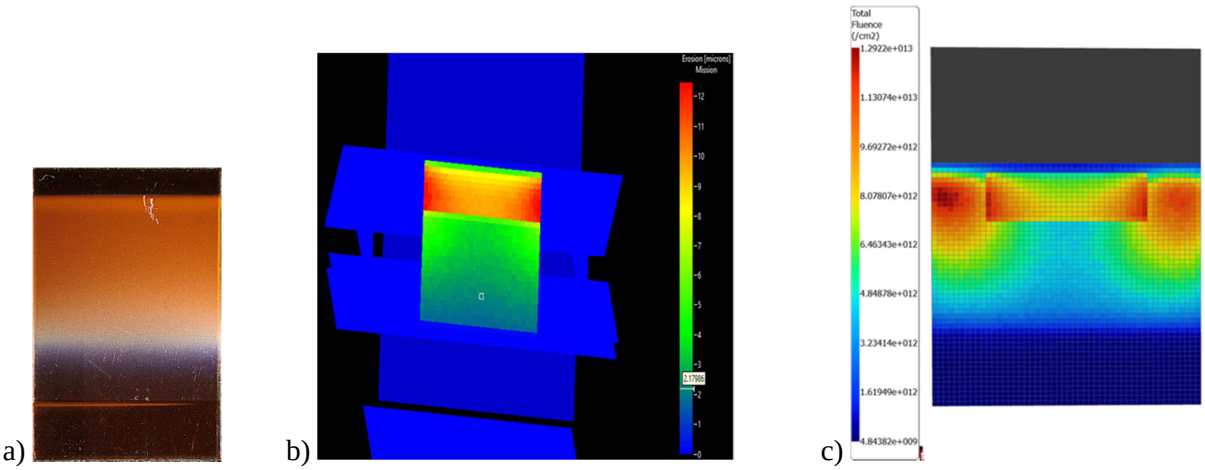

Figure 16. a. Optical eroded pattern (PCC reflector). Computed eroded pattern (**b**: ESABASE2; **c**: SYSTEMA).

It can be concluded that eroded pattern could be fairly well reproduced by simulation tools. Nonetheless, this work only describes a rough reproduction of the experimental results. A better

methodology should be thought of to improve the accuracy of the simulations. In particular another check point concerns the total mass loss whose discrepancy between computed and experimental values remains in the range 8 to 40 % in this first approach.

5. Conclusions and perspectives

In this work, an original geometrical setup was designed in order to expose target surfaces with normal incidence or after one reflection. Candidate materials have been selected in view to compare numerical results conducted with usual modeling tools and experimental results. As already mentioned in the literature, Kapton HN was confirmed as a reference material to evaluate the level of fluence during the test campaign. Its erosion yield was confirmed to be independent of the impingement angle θ, by using the effective fluence ('cos(θ)' correction factor). Concerning the geometrical effect, all the materials tested with a 65°-impingement angle seem more sensitive to inclined AO erosion than normal-oriented erosion. After reflection on the inclined-MUT samples, the residual fluence coming on the detector surface is about one tenth of the direct incident fluence. The Coverglass is the more reflective material with ~10 % of secondary fluence, other materials are between 4 and 10 %. From the optical observation of eroded Kapton films used as detectors, it's clear the erosion area includes the area of specular reflection as well as a more or less large diffuse reflection area, the size and the form being dependent on the reflective materials nature. First computations with industrial codes implementing AO erosion process with multiple reflections have been successfully conducted, the erosion patterns being rather well described with some basic hypotheses on material parameters and taken into account the reflection on metallic sides, in order to reproduce the concave shape between eroded and non-eroded areas.

The first perspective will be to improve the modeling method with a parameters optimization based on the total mass loss and the use of multiple points of control with extracted erosion depths from the profilometry measurements. Moreover a near future goal is to apply this modeling to SESAME geometries (being part of the ESA Bartolomeo platform for material space experiment onboard the ISS) and compare ground vs flight data.

Acknowledgments

The authors would like to acknowledge the ESA-ESTEC technical staff for their helpful work at LEOX facility and the financial support from CNES R&T program and ADS and TAS co-funding.

References

[1] Crisp N H *et al.* 2021 System modelling of very low Earth orbit satellites for Earth observation *Acta Astronautica* **187** pp 475–491

[2] Banks B A, Miller S K R, de Groh K K and Demko R 2003 Scattered Atomic Oxygen Effects on Spacecraft Materials *Proceedings of the 9th International Symposium on Materials in a Space Environment* ESA SP-540 Noordwijk The Netherlands pp 145–152

[3] Banks B A, de Groh K K, Miller S K and Waters D L 2008 Lessons Learned From Atomic Oxygen Interaction With Spacecraft Materials in Low Earth Orbit *NASA Technical Memorandum* NASA/TM—2008-215264

[4] Bourassa R J and Gillis J R 1991 LDEF Atomic Oxygen Fluence Update LDEF Materials Workshop '91 NASA Conference Publication 3162 Part 1 pp 59-69

[5] Kimoto Y, Shimabukuro T, Sakai M and Koizumi T 2015 Simulation of Atomic Oxygen Behavior Using the NC-DSMC Method in Combined Space Effects Test Facility *Proceedings of the 13th ISMSE*, Pau, France, 22-26 June 2015

[6] Duzellier S, Lévêque D, Pons C, Soonckindt S, Laurent E, Chanteperdrix G, Vilaranda-Fernandez M, Jouanne P, Perrin-Bailly V and Nguyen Van Sang D 2021 Ground investigation of AO effect in case of complex geometry *Proceedings of the 1st International Symposium on very low earth orbit missions and technologies*, Virtual Event, 28-29 June 2021

[7] Banks B A and Miller S K 2018 Effects of Sample Holder Edge Geometry on Atomic Oxygen Erosion Yield of Pyrolytic Graphite Exposed in Low Earth Orbit *NASA Technical Memorandum* NASA/TM—2018-219910
[8] Banks B A, Seroka K T, McPhate J B and Miller S K 2011 Attenuation of Scattered Thermal Energy Atomic Oxygen *NASA Technical Memorandum* NASA/TM—2011-217028
[9] Duzellier S, Soonckindt S, Chardon J P, Pons C, Laurent E, Remaury S, Minton T and Murray V 2018 Validation of Atomic Oxygen Active Detector Resistack *Proceedings of the 14th ISMSE & 12th ICPMSE* Biarritz France 1 to 5 October 2018
[10] Yokota K, Tagawa M, and Ohmae N 2002 Impingement Angle Dependence of Erosion Rate of Polyimide in Atomic Oxygen Exposures *J Spacecraft* **39** NO.1: Engineering Notes pp 155-156
[11] Minton T K 1995 Protocol for Atomic Oxygen Testing of Materials in Ground-Based Facilities Version Number 2 *JPL Publication* 95-17
[12] Banks B A, Waters D L, Thorson S D, de Groh K K, Snyder A and Miller S 2006 Comparison of Atomic Oxygen Erosion Yields of Materials at Various Energy and Impact Angles *NASA Technical Memorandum* NASA/TM—2006-214363
[13] Banks B A et al. 1992 Monte Carlo Modeling of Atomic Oxygen Interaction with Protected polymers for Projection of Materials Durability in Low Earth Orbit *Mat. Res. Soc.* **278**
[14] Chen L and Lee C-H 2006 Interaction potential between atomic oxygen and polymer surfaces in low earth orbit *Journal of Spacecraft and Rockets* **43** n°3